Energy-efficient Ring Formation Control with Constrained Inputs

Praveen Kumar Ranjan *, Abhinav Sinha†, and Yongcan Cao ‡.
Unmanned Systems Lab, Department of Electrical and Computer Engineering,
The University of Texas at San Antonio, San Antonio, TX, 78249

Dzung Tran§, David Casbeer¶, and Isaac Weintraub‖
Control Science Center, U.S. Air Force Research Laboratory,
Wright-Patterson Air Force Base, OH, 45433.

I. Introduction

Multivehicle missions have rapidly gained popularity due to their widespread use in a variety of applications, e.g., [1–4]. A typical problem in the area of multivehicle cooperative control is formation control, wherein a group of vehicles form up and move in a specified geometrical shape. Among various formation techniques, leader-follower formation is of specific interest since the leader's behavior can directly influence that of the followers [5, 6]. While maintaining a rigid formation is crucial for applications like target triangulation, and surveillance [7, 8], having a flexible formation geometry may be of particular importance in area mapping, search and rescue, transportation, etc.

In literature, formation control based on simplified models has been used widely to address leader-follower formation flying, where the follower agents maintain a fixed relative configuration with respect to the leader [9–12]. In [9], a leader-follower formation feedback controller based on distance and bearing information of the leader was developed by considering the planar kinematics model to control the velocity and turning rate of the follower. The proportional-integral formation controller of [10] had two decoupled autopilots to independently control the heading and the speed of the follower modeled as a first-order system. In [11], two-dimensional guidance laws were developed for leader-follower formation flight utilizing the line of sight information. In [12], the formation control laws were derived using system identification on flight data to maintain the specified geometry.

The virtual structure method is another popular choice for solving the formation flying problem where the vehicles' trajectories are generated based on virtual formation structure [13–18]. This method provides flexibility in maintaining formation through the vehicles' variable relative configuration. In [14], independent heading, altitude, and airspeed controllers were developed to maintain flexible virtual structure formation using planar kinematics. The design was

*Graduate Student, email: praveen.ranjan@my.utsa.edu.
†Postdoctoral Research Fellow, email: abhinav.sinha@utsa.edu.
‡Associate Professor, email: yongcan.cao@utsa.edu. ‡ Corresponding author
§Research Associate, email: dzung.tran.ctr@afrl.af.mil
¶Team Lead, david.casbeer@us.af.mil.
‖Electronics Engineer, isaac.weintraub.1@us.af.mil.
Distribution A: Approved for public release. Case #: AFRL-2022-2827.
This manuscript is also accepted for presentation at the AIAA SciTech Forum 2023 to be held from Jan 23 to 27, 2023 at MD, USA.

further implemented on a six-degree-of-freedom model of a fixed-wing aircraft. The work in [15] discussed a flexible formation control that minimizes the impact of rotation structures when the leader changes its heading. In [16], two independent vertical and horizontal direction controllers were developed where kinetic and potential energy can be exchanged to meet the desired velocity or altitude requirement. This was achieved by considering a virtual formation structure based on the aircraft's velocity or altitude.

Note that most studies, including the aforementioned ones, only considered the follower's fixed relative configuration with respect to the leader. There are, however, a few works that have addressed the leader-follower flexible formation control. Motivated by the formation strategy used by the pilots [19], the authors in [20–22] proposed to achieve a ring formation around the leader. Instead of maintaining a rigid formation with respect to the leader, the follower can now converge to a ring around it. Two different strategies were proposed in this regard. The first one presented an explicit control law that defines a point on the ring and updates it depending on the current position of the follower. The second one used a potential field method in the context of an aircraft modeled using first-order dynamics. The authors in [21, 22] designed the follower's acceleration using nonlinear design techniques considering higher-order aircraft dynamics for ring formation.

The follower's energy expenditure is also crucial to consider from a practical standpoint since the amount of fuel consumption is related to the drag acting on the vehicle [23, 24]. For example, the authors in [16, 25, 26] designed controllers to quantify and minimize the energy expenditure during flight. These controllers allowed the exchange between the potential energy and the kinetic energy of the follower aircraft to maintain the desired speed or altitude, which cannot be controlled independently. The authors in [16] utilized a controller based on energy maneuverability to analyze the fuel consumption in formation flight. In particular, the controller therein consumed less fuel while using the vehicle's thrust as the main input to change its altitude for formation flight. For flexible formation flight, the work in [27] optimized the thrust consumption of the follower aircraft by making it converge to a specific point on the ring behind the maneuvering leader. This specific point on the ring was obtained such that the follower's thrust consumption was minimized if converging to that point. These studies show that the thrust applied to steer an aircraft is related to its fuel consumption and serves as an important performance index quantifying the energy usage of the aircraft.

In this paper, we extend the previous studies on ring formation by considering the higher-order dynamic model of the leader-follower system while aiming to minimize the follower's energy expenditure. The main contribution of this paper is to propose a novel energy-efficient flexible leader-follower formation. This choice is motivated by the fact that introducing flexibility in leader-follower formation could potentially lead to wide-area monitoring, inter-vehicle safety in a complicated environment, and reduced maneuverability requirements for the follower. For consistency, we also refer to the proposed leader-follower formation as the follower's ring formation around the leader, as done in our previous work, [27]. Most existing works do not consider minimizing the follower's energy in a formation as it adds to the complexity of the formation control problem. In the proposed formation, the follower's position is not rigidly fixed with respect to the

leader; rather, it is steered to a certain point on the ring. Unlike [27], where the desired point on the ring was obtained as a solution to the optimization problem, we aim to steer the follower to a specific point on the ring, namely, the minimum speed point, in order to lower the follower's energy expenditure. Further, the computation of the minimum energy point is analytical in the present work. In [27], open-loop energy optimal solutions for the ring formation problem were obtained utilizing a finite horizon optimizer. However, in the current work, we obtain an energy-efficient feedback controller using the backstepping technique. Additionally, the proposed approach designates the follower's thrust, load factor, and bank angle as its control inputs, unlike existing studies that do not directly manipulate these variables to control the follower's position. While we used an optimizer to constrain the control inputs in [27], we account for the follower's inherent limits on the available control effort in the design using nonlinear programming. We also show that it can be steered to the minimum energy point on the ring from various initial configurations relative to the leader.

We adopt the following notations throughout this paper. Lowercase boldfaced letters represent vectors, while uppercase boldfaced letters denote matrices. The transpose of a vector/matrix is represented by a $(\cdot)^\top$ and $(\cdot)^{-1}$ denotes the inverse of a matrix. The coordinate axes are represented by $[X_{(\cdot)}, Y_{(\cdot)}, Z_{(\cdot)}]^\top$, where the origin of that frame of reference is at $(\cdot)$. The maximum and minimum eigenvalue of a matrix are represented using $\lambda_{\max}(\cdot)$ and $\lambda_{\min}(\cdot)$, respectively. Similarly, $\mathbb{R}^n$ and $\mathbb{R}^{n\times m}$, respectively, denote the vectors and matrices of appropriate dimensions in real Euclidean space, where n, m are natural numbers. The Euclidean norm of a vector is denoted by a $\|\cdot\|_2$.

II. Background and Problem Formulation

We consider leader and follower aircraft whose kinematics is given by

$$\dot{x}_k(t) = V_k(t)\cos\gamma_k(t)\cos\chi_k(t),\ \dot{y}_k(t) = V_k(t)\cos\gamma_k(t)\sin\chi_k(t),\ \dot{z}_k(t) = -V_k(t)\sin\gamma_k(t), \tag{1}$$

where the subscript $k \in \{l, f\}$ represents either the leader or the follower aircraft. The position of the k^{th} aircraft in the inertial frame is denoted by $\mathbf{p}_k = [x_k, y_k, z_k]^\top$, such that $\dot{\mathbf{p}}_k = [\dot{x}_k, \dot{y}_k, \dot{z}_k]^\top$ is its velocity in the same frame. For $[X_I, Y_I, Z_I]^\top$ denoting the inertial frame, $V_k(t)$, $\gamma_k(t)$, and $\chi_k(t)$ denote the velocity, the flight path angle, and the heading angle of the respective aircraft, whose dynamics are governed by the following set of equations:

$$\dot{V}_k(t) = \frac{T_k(t) - D_k(t)}{m_k} - g\sin\gamma_k(t), \dot{\gamma}_k(t) = \frac{g}{V_k(t)}\left(n_k(t)\cos\phi_k(t) - \cos\gamma_k(t)\right), \dot{\chi}_k(t) = \frac{g}{V_k(t)}\left(\frac{n_k(t)\sin\phi_k(t)}{\cos\gamma_k(t)}\right), \tag{2}$$

where m_k, $T_k(t)$, $n_k(t)$, and $\phi_k(t)$ denote the mass, the thrust, the load factor, and the bank angle of the k^{th} aircraft, respectively. The drag acting on the k^{th} aircraft can be estimated from the drag polar as $D_k(t) = \frac{1}{2}\rho V_k(t)^2 A_k\left(C_{d_{0_k}}(t) + C_{d_{i_k}}(t)\right)$, where $C_{d_{0_k}}$ is the parasitic drag coefficient, $C_{d_{i_k}}$ is the induced drag, such that

$C_{d_{i_k}} = \dfrac{C_{l_k}^2(t)}{\pi A_{r_k} \eta_k}$, and $C_{l_k} = \dfrac{2 n_k m_k g}{\rho {V_k}^2 A_k}$ is the lift coefficient, which depends on aerodynamic parameters, e.g., aspect ratio A_{r_k}, wing surface area A_k, Oswald's efficiency ratio η_k, and the acceleration due to gravity g. Instead of getting into much detail here, we refer readers to [28] for details on these aerodynamic parameters. It is important to note that the total specific energy, E, and the specific power, P for an aircraft, as derived in [29], are given by $E = \dfrac{1}{2} V_k^2 - g\, z_k$ and $P = \dfrac{V_k (T_k - D_k)}{m_k}$. It is evident that the energy expenditure is related to the aircraft speed, thrust, and drag. Hence, it is expected that minimizing these variables may lead to less energy expenditure.

Unlike most studies, e.g., [30–37], which use the vehicle's fin deflections, heading, turn rate, or acceleration to control its position, we propose to directly manipulate its thrust, load factor, and bank angle to control its position since these variables may be more realistic, and are directly related to vehicle's energy consideration. Therefore, from (1)–(2), it is apparent that the dynamics of the aircraft's position has a relative degree of two with respect to the designated control inputs– thrust, load factor, and bank angle, such that

$$\begin{aligned}
\ddot{x}_k &= \left(\frac{T_k - D_k}{m}\right) \cos\gamma_k \cos\chi_k - n_k g \left(\sin\gamma_k \cos\chi_k \cos\phi_k + \sin\chi_k \sin\phi_k\right) \\
\ddot{y}_k &= \left(\frac{T_k - D_k}{m}\right) \cos\gamma_k \sin\chi_k - n_k g \left(\sin\gamma_k \sin\chi_k \cos\phi_k - \cos\chi_k \sin\phi_k\right) \\
\ddot{z}_k &= -\left(\frac{T_k - D_k}{m}\right) \sin\gamma_k - n_k g \left(\cos\gamma_k \cos\phi_k\right) + g,
\end{aligned} \tag{3}$$

where we have now dropped the arguments of the variables for brevity, and considered $m_k = m$, since we assume that the leader and the follower aircraft are homogeneous. Alternately, we can represent (3) compactly as $\ddot{\mathbf{p}}_k(t) = [\ddot{x}_k(t), \ddot{y}_k(t), \ddot{z}_k(t)]^\top$ to denote the acceleration of the k^{th} aircraft in the inertial frame.

This paper also considers the limits on the vehicles' available control efforts since their thrust, load factor, and bank angle are constrained and bounded in practice. To this aim, we consider a mathematically convenient second-order dynamics with constrained inputs, using (1)–(2), $\ddot{\mathbf{p}}_k = \mathbf{B}_k(t)\, \text{sat}(\tilde{\mathbf{u}}_k(t)) + \mathbf{g}$, where

$$\mathbf{B}_k(t) = \begin{bmatrix} \cos\gamma_k \cos\chi_k & -\sin\gamma_k \cos\chi_k & -\sin\chi_k \\ \cos\gamma_k \sin\chi_k & -\sin\gamma_k \sin\chi_k & \cos\chi_k \\ -\sin\gamma_k & -\cos\gamma_k & 0 \end{bmatrix}, \ \mathbf{g} = \begin{bmatrix} 0 \\ 0 \\ g \end{bmatrix}, \ \tilde{\mathbf{u}}_k(t) = \begin{bmatrix} \dfrac{T_k - D_k}{m} \\ n_k \cos\phi_k \\ n_k \sin\phi_k \end{bmatrix}, \tag{4}$$

with T_k, n_k and ϕ_k being the actual control inputs. Since $\mathbf{B}_k$ is of full rank, there is no loss of controllability. The control inputs in our design are constrained within their physical limits using a nonlinear programming routine and is denoted by a saturation function. In this paper, we consider the problem of controlling the position of the follower aircraft in a flexible formation. While the leader is free to make independent maneuvers, the follower needs to converge to a virtual ring around the leader. We call it the follower's ring formation maneuver for simplicity. This virtual ring

around the leader represents an infinite set of desired trajectories for the follower to converge on, thus eliminating the need for the leader-follower system to maintain a rigid formation. The follower can now choose to converge to any point on the ring, which may not be possible in rigid formations. However, our objective here is to steer the follower to a specific point on the ring that corresponds to minimum energy expenditure, using practical control inputs (thrust, load factor, and bank angle), thereby making the leader-follower formation energy-efficient and implementable in practice.

III. Energy-efficient Leader-follower Ring Formation

In this section, we first derive the specific point on the ring that corresponds to the follower's minimum energy expenditure, followed by the suitable control inputs to steer it to that point on the ring from arbitrary initial positions. Fig. 1 depicts the leader-follower aircraft system where a red-colored virtual ring is attached to the leader aircraft. Their body-fixed frames are $[X_{l_B}, Y_{l_B}, Z_{l_B}]^\top$ and $[X_{f_B}, Y_{f_B}, Z_{f_B}]^\top$, whereas the frame $[X_{r_B}, Y_{r_B}, Z_{r_B}]^\top$ represents the body frame of center of the ring. The frames attached to the leader and center of the ring are always parallel, separated by an offset along the body X-axis as the ring is rigidly attached. For our convenience, we have chosen the body-fixed and inertial coordinate frames with a downward-facing Z-axis. The X and Y-axes are chosen accordingly to complete the right-handed coordinate system. Note that the thrust required to maintain a steady flight is related to the follower's

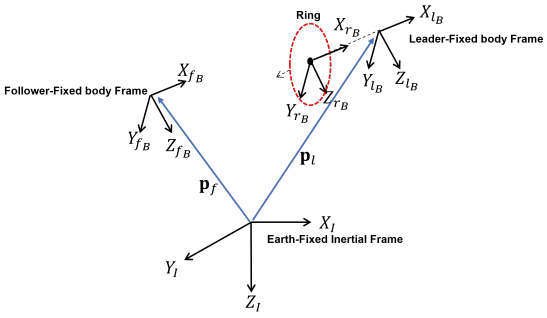

Fig. 1 The leader-follower ring formation geometry.

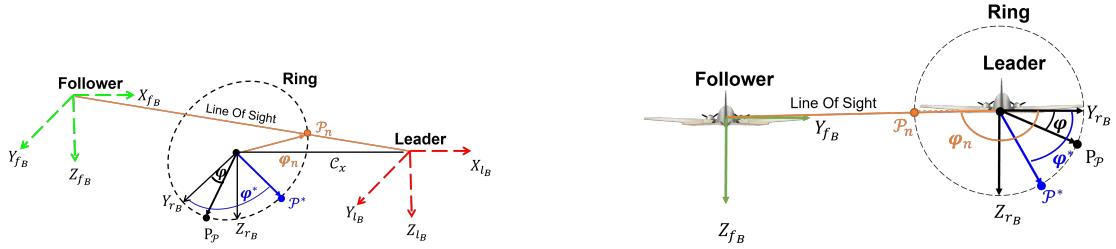

(a) Isometric view of the ring. **(b) Back/planar view of the ring.**

Fig. 2 Virtual ring behind the leader.

energy expenditure since the thrust and the drag are balanced in the steady state. Thus, lower thrust will require less drag to balance it, resulting in less energy consumption.

A. Minimum Energy Point on the Virtual Ring

Consider a virtual ring located behind the leader at a certain distance, as shown in Fig. 2. The ring, whose radius is R, is centered at (C_x, C_y, C_z), as seen in the leader's body frame. Since the ring is located directly behind the leader and separated by an offset of C_x, it is clear that $C_y = C_z = 0$ since their body frames are parallel to each other. We further assume that R and C_x remain invariant throughout the formation.

Let us now consider a point on the ring, $\mathcal{P}$, such that the ring angle, φ, is the angle subtended by the line joining $\mathcal{P}$ and the $y-$axis in the leader's frame, measured counterclockwise, by assuming that the leader's heading is aligned with its body x-axis. Note that the ring's frame is rigidly attached to the leader's body frame. Hence, the velocity experienced at any point in the ring, $\mathbf{V}_{\mathcal{P}}$, is the sum of the leader's velocity, $\mathbf{V}_l$, and an additional term that depends on the leader's angular velocity, $\boldsymbol{\omega}_l$, and the offset from its center of mass, $\mathbf{r}_{\mathcal{P}}$, given by

$$\mathbf{V}_{\mathcal{P}} = \mathbf{V}_l + \boldsymbol{\omega}_l \times \mathbf{r}_{\mathcal{P}} = \begin{bmatrix} V_l + \dot{\gamma}_l(C_z + R\sin\varphi) - \dot{\chi}_l(C_y + R\cos\varphi) \\ R\dot{\chi}_l \\ -R\dot{\gamma}_l \end{bmatrix}; \mathbf{V}_l = [V_l, 0, 0]^\top, \boldsymbol{\omega}_l = [0, \dot{\gamma}_l, \dot{\chi}_l]^\top \tag{5}$$

and $\mathbf{r}_{\mathcal{P}} = \left[C_x, C_y + R\cos\varphi, C_z + R\sin\varphi\right]^\top$. We can now use rotation matrices to obtain the position of any point on the ring in the inertial frame, $\mathbf{p}_{\mathcal{P}}$, as $\mathbf{p}_{\mathcal{P}} = \mathbf{p}_l + \mathbf{R}(\gamma_l, \chi_l)\mathbf{r}_{\mathcal{P}}$, where $\mathbf{R}(\gamma_l, \chi_l) = \begin{bmatrix} \cos\chi_l & -\sin\chi_l & 0 \\ \sin\chi_l & \cos\chi_l & 0 \\ 0 & 0 & 1 \end{bmatrix}\begin{bmatrix} \cos\gamma_l & 0 & \sin\gamma_l \\ 0 & 1 & 0 \\ -\sin\gamma_l & 0 & \cos\gamma_l \end{bmatrix}$ denotes the composite rotation matrix that transforms a vector from the leader's body frame to the inertial frame.

In general, the follower can converge to any point, $\mathcal{P}$, on the ring, thereby making it critical to determine which point to stay at with respect to the leader's specific position and heading at a particular time. We consider steering the follower on a specific point on the ring, $\mathcal{P}^\star$, such that its speed is minimum since moving slowly essentially means applying small acceleration, which requires less thrust. For example, when the leader moves in a straight line, all points on the ring have the same velocity, equal to that of the leader. Consequently, convergence to any point on the ring will require equal thrust. However, when the leader performs a different maneuver from a straight line, the points on the ring have different velocities depending on the leader's angular velocity. Since the point with less speed means less thrust, it is important to provide an analytic study of the point with minimum speed.

Lemma 1. *A point on the ring, $\mathcal{P}^\star$, has minimum speed if it subtends a ring angle,*

$$\varphi^\star = \tan^{-1}\left(\frac{-\dot{\gamma}_l}{\dot{\chi}_l}\right);\ \dot{\gamma}_l \neq 0,\ \dot{\chi}_l \neq 0, \tag{6}$$

with respect to the $Y-$axis in the leader's body frame.

Proof. Since minimizing the velocity, namely, the magnitude of $\mathbf{V}_{\mathcal{P}}$, is equivalent to minimizing $\frac{1}{2}\mathbf{V}_{\mathcal{P}}^{\top}\mathbf{V}_{\mathcal{P}}$, we begin by differentiating $\mathbf{V}_{\mathcal{P}}$ with respect to φ and set it equal to zero, that is,

$$\frac{1}{2}\frac{\partial}{\partial\varphi}\left(\mathbf{V}_{\mathcal{P}}^{\top}\mathbf{V}_{\mathcal{P}}\right)=0 \implies \mathbf{V}_{\mathcal{P}}^{\top}\frac{\partial\mathbf{V}_{\mathcal{P}}}{\partial\varphi}=0, \tag{7}$$

which can be further simplified, using, (5), as

$$\begin{bmatrix} V_l+\dot{\gamma}_l(C_z+R\sin\varphi)-\dot{\chi}_l(C_y+R\cos\varphi) & C_x\dot{\chi}_l & -C_x\dot{\gamma}_l \end{bmatrix}^{\top}\begin{bmatrix} R\dot{\gamma}_l\cos\varphi+R\dot{\chi}_l\sin\varphi \\ 0 \\ 0 \end{bmatrix}=0. \tag{8}$$

Equivalentally, from (8), one has $\left(V_l+\dot{\gamma}_l(C_z+R\sin\varphi)-\dot{\chi}_l(C_y+R\cos\varphi)\right)\left(R\dot{\gamma}_l\cos\varphi+R\dot{\chi}_l\sin\varphi\right)=0$ whose two solutions are $\varphi=\tan^{-1}\left(\frac{-\dot{\gamma}_l}{\dot{\chi}_l}\right)$, and $\varphi=\tan^{-1}\left(\frac{\dot{\gamma}_l}{-\dot{\chi}_l}\right)$. Evaluating $\frac{1}{2}\frac{\partial^2}{\partial\varphi^2}\left(\mathbf{V}_{\mathcal{P}}^{\top}\mathbf{V}_{\mathcal{P}}\right)$ at (6) results in

$$\begin{aligned}\frac{1}{2}\frac{\partial^2}{\partial\varphi^2}\left(\mathbf{V}_{\mathcal{P}}^{\top}\mathbf{V}_{\mathcal{P}}\right)\Big|_{\varphi=\varphi^*} &= \left(R\dot{\gamma}_l\cos\varphi+R\dot{\chi}_l\sin\varphi\right)^2+\left(V_l+R\dot{\gamma}_l\sin\varphi-R\dot{\chi}_l\cos\varphi\right)\left(-R\dot{\gamma}_l\sin\varphi+R\dot{\chi}\cos\varphi\right)\Big|_{\varphi=\varphi^*}\\ &= \left(V_l-R\sqrt{\dot{\gamma}_l^2+\dot{\chi}_l^2}\right)\left(R\sqrt{\dot{\gamma}_l^2+\dot{\chi}_l^2}\right).\end{aligned} \tag{9}$$

From (9), it is apparent that $\frac{1}{2}\frac{\partial^2}{\partial\varphi^2}\left(\mathbf{V}_{\mathcal{P}}^{\top}\mathbf{V}_{\mathcal{P}}\right)\Big|_{\varphi=\varphi^*}>0$ since the leader's speed cannot be negative. Thus, it readily follows that (6) corresponds to the minimum. □

Recall that the follower needs to converge to $\varphi^{\star}$ irrespective of the leader's maneuver. However, if the leader moves in a straight line, then one may observe from Lemma 1 that $\dot{\gamma}_l=\dot{\chi}_l=0$. This particular scenario may lead to inconsistencies in the definition of $\varphi^{\star}$ in (6), whose investigation is our next objective.

If the leader moves in a straight line, then $\mathbf{V}_{\mathcal{P}}=\mathbf{V}_l=[V_l,0,0]^{\top}$. This essentially means that any $\mathcal{P}$ can correspond to the point of minimum energy. Thus, the follower may choose to converge to the nearest point on the ring, say $\mathcal{P}_n$, given by

$$\varphi=\tan^{-1}\left(\frac{C_z-\mathbf{e}_3^{\top}\mathbf{R}^{\top}(\gamma_l,\chi_l)\mathbf{p}_f}{C_y-\mathbf{e}_2^{\top}\mathbf{R}^{\top}(\gamma_l,\chi_l)\mathbf{p}_f}\right), \tag{10}$$

where $\mathbf{e}_2,\mathbf{e}_3$ are the standard bases in $\mathbb{R}^3$. This computation of (10) in our paper is also consistent with the one in [38]. Since the follower's nearest point on the ring may change, it may show a tendency to abruptly jump to another $\mathcal{P}$ than the one it was initially aiming at. To prevent a sudden jump in the follower's trajectory and control inputs, the rate of change of the ring angle can be regulated via some desired dynamics. For example, letting $\dot{\varphi}^{\star}-\dot{\varphi}=-\kappa\left(\varphi^{\star}-\varphi\right)$ for

some $\kappa > 0$ would allow the follower a smooth transition among nearest points at different instants of time.

B. The Follower's Control Law

Having computed the specific point at which the follower needs to converge, we now present the proposed control law in this subsection. Consider the error between the position of the follower aircraft and the point of minimum energy on the ring in inertial frame,

$$\mathbf{e} = \mathbf{p}_f - \mathbf{p}_{\mathcal{P}^\star} = \mathbf{p}_f - \mathbf{p}_l - \mathbf{R}(\gamma_l, \chi_l)\mathbf{r}_{\mathcal{P}^\star}, \tag{11}$$

where $\mathbf{p}_{\mathcal{P}^\star}$ and $\mathbf{r}_{\mathcal{P}^\star}$ are the same as in $\mathbf{p}_{\mathcal{P}}$ and $\mathbf{r}_{\mathcal{P}}$ defined previously, except that a $\star$ indicates that they corresponds to $\mathcal{P}^\star$. Since the system under consideration has a relative degree of two, time differentiating (11) twice yields

$$\ddot{\mathbf{e}} = \ddot{\mathbf{p}}_f - \ddot{\mathbf{p}}_l - \frac{d^2}{dt^2}\left(\mathbf{R}(\gamma_l, \chi_l)\mathbf{r}_{\mathcal{P}^\star}\right), \tag{12}$$

which can be written as a second-order nonlinear system with a bounded uncertainty, that is,

$$\ddot{\mathbf{e}} = \mathbf{B}_f\,\mathrm{sat}(\tilde{\mathbf{u}}_f) + \mathbf{g} + \mathbf{d};\ \mathbf{d} = -\ddot{\mathbf{p}}_l - \frac{d^2}{dt^2}\left(\mathbf{R}(\gamma_l, \phi_l)\mathbf{r}_{\mathcal{P}^\star}\right). \tag{13}$$

Remark 1. The term $\mathbf{d}$ represents the second derivative of the position of the minimum speed point in the inertial frame. The position of the minimum speed point can be obtained using a combination of sensors mounted on the follower as well as being aided by a ground station, which can communicate some of the leader's information (e.g., its heading angles and turn rates) to the follower. We treat $\mathbf{d}$ as an uncertainty since evaluating its analytical expression may be cumbersome, and higher-order derivatives of $\mathcal{P}^*$ may not be available for measurement directly. Instead, we resort to using command filters [39] to obtain an estimate of $\mathbf{d}$, say $\hat{\mathbf{d}}$, which may be favorable in such scenarios. Also, this helps us to simplify the equation 12 by grouping together the terms not directly computable by the follower under a single uncertain variable $\mathbf{d}$.

For convenience, let us write (13) as

$$\dot{\mathbf{z}}_1 = \mathbf{z}_2 \tag{14a}$$

$$\dot{\mathbf{z}}_2 = \mathbf{B}_f\,\mathrm{sat}(\tilde{\mathbf{u}}_f) + \mathbf{g} + \hat{\mathbf{d}}, \tag{14b}$$

where $\hat{\mathbf{d}}$ is an approximation of $-\ddot{\mathbf{p}}_l - \frac{d^2}{dt^2}\left(\mathbf{R}(\gamma_l, \chi_l)\mathbf{r}_{\mathcal{P}^\star}\right)$. In (14), we denote $\mathbf{e}$ and $\dot{\mathbf{e}}$ by $\mathbf{z}_1$ and $\mathbf{z}_2$, respectively. Our goal here is to stabilize $\mathbf{z}_1$ and $\mathbf{z}_2$ to the origin with suitable control input, $\tilde{\mathbf{u}}_f$, respecting the saturation constraints which, in essence, is equivalent to designing the follower's necessary thrust, load factor, and bank angle. At this stage, we recall

that the actual control input, $\mathbf{u}_f = [T_f, n_f, \phi_f]^\top$, is related to $\tilde{\mathbf{u}}_f$ as

$$u_{f_1} = T_f = m\tilde{u}_{f_1} + D_f, \tag{15a}$$

$$u_{f_2} = n_f = \sqrt{\tilde{u}_{f_2}^2 + \tilde{u}_{f_2}^2}, \tag{15b}$$

$$u_{f_3} = \phi_f = \tan^{-1}\frac{\tilde{u}_{f_3}}{\tilde{u}_{f_2}}. \tag{15c}$$

Theorem 1. *Consider the error dynamics* (13) *and the auxiliary nonlinear system,* (14)*. If the control input for the system* (14) *is designed as*

$$\tilde{\mathbf{u}}_f = -\mathbf{B}_f^{-1}\left(-\mathbf{N}\boldsymbol{\zeta} - \mathbf{g} - \hat{\mathbf{d}} - \mathbf{K}\mathbf{z}_2 + \mathbf{M}\boldsymbol{\xi} - \mathbf{z}_1\right), \tag{16}$$

where $\boldsymbol{\xi}$ *is obtained via*

$$\dot{\boldsymbol{\xi}} = -\mathbf{M}\boldsymbol{\xi} + \mathbf{B}_f\left(\tilde{\mathbf{u}}_f - \text{sat}(\tilde{\mathbf{u}}_f)\right) \tag{17}$$

and is related to $\boldsymbol{\zeta}$ *through*

$$\boldsymbol{\zeta} = \mathbf{z}_2 + \mathbf{K}\mathbf{z}_1 + \boldsymbol{\xi}, \tag{18}$$

such that $\mathbf{K}, \mathbf{M}, \mathbf{N}$ *are diagonal matrices of appropriate dimensions having positive entries, then the trajectories of* (14) *remain uniformly bounded within a compact set,*

$$\Omega = \left\{ (\mathbf{z}_1, \boldsymbol{\zeta}) \;:\; \|\mathbf{z}_1\|_2 \leq \frac{\|\boldsymbol{\xi}\|_2}{\lambda_{\max}(K)},\; \|\boldsymbol{\zeta}\|_2 \leq \frac{\left\|\left(\mathbf{d} - \hat{\mathbf{d}}\right)\right\|_2}{\lambda_{\max}(N)} \right\}, \tag{19}$$

with an ultimate performance bound,

$$\|\mathbf{z}_1\|_2 \leq \max_{(\mathbf{z}_1, \boldsymbol{\zeta}) \in \Omega} \sqrt{\left(\frac{\boldsymbol{\xi}}{\lambda_{\max}(K)}\right)^2 + \left(\frac{\mathbf{d} - \hat{\mathbf{d}}}{\lambda_{\max}(N)}\right)^2}. \tag{20}$$

Proof. Consider a Lyapunov function candidate, $W_1(\mathbf{z}_1) = \frac{1}{2}\mathbf{z}_1^\top \mathbf{z}_1$, whose time differentiation results in $\dot{W}_1(\mathbf{z}_1) = \mathbf{z}_1^\top \mathbf{z}_2$. If we let $\mathbf{z}_2 = -\mathbf{K}\mathbf{z}_1$, then the origin of the system, $\dot{\mathbf{z}}_1 = -\mathbf{K}\mathbf{z}_1$, is asymptotically stable. We now use the backstepping technique to account for saturation constraints on the control input. To this aim, we consider an intermediate relationship, (18), such that $\boldsymbol{\xi}$ compensates the effects of input saturation, and whose dynamics is given as (17).

One may observe from (17) that if $\tilde{\mathbf{u}}_f$, and hence the follower's control law, respects the saturation constraints, then $\boldsymbol{\xi}$ decays to zero asymptotically since $\tilde{\mathbf{u}}_f - \text{sat}(\tilde{\mathbf{u}}_f)$ is ideally zero in that scenario.

Now we consider another Lyapunov function candidate, $W_2(\mathbf{z}_1, \boldsymbol{\zeta}) = W_1(\mathbf{z}_1) + \frac{1}{2}\boldsymbol{\zeta}^\top\boldsymbol{\zeta} = \frac{1}{2}\mathbf{z}_1^\top\mathbf{z}_1 + \frac{1}{2}\boldsymbol{\zeta}^\top\boldsymbol{\zeta}$. Differentiating

$W_2(\mathbf{z}_1, \boldsymbol{\zeta})$ with respect to time, and using (18) and (17), yields

$$\dot{W}_2(\mathbf{z}_1, \boldsymbol{\zeta}) = \mathbf{z}_1^\top \left(\boldsymbol{\zeta} - \mathbf{K}\mathbf{z}_1 - \boldsymbol{\xi}\right) + \boldsymbol{\zeta}^\top \dot{\boldsymbol{\zeta}} = -\mathbf{z}_1^\top \left(\boldsymbol{\zeta} - \mathbf{K}\mathbf{z}_1 - \boldsymbol{\xi}\right) + \boldsymbol{\zeta}^\top \left[\dot{\mathbf{z}}_2 + \mathbf{K}\mathbf{z}_2 - \mathbf{M}\boldsymbol{\xi} + \mathbf{B}_f \left(\tilde{\mathbf{u}}_f - \text{sat}(\tilde{\mathbf{u}}_f)\right)\right]. \tag{21}$$

Simplifying (21) further, using (14), results in

$$\begin{aligned}
\dot{W}_2(\mathbf{z}_1, \boldsymbol{\zeta}) &= -\mathbf{z}_1^\top \left(\boldsymbol{\zeta} - \mathbf{K}\mathbf{z}_1 - \boldsymbol{\xi}\right) + \boldsymbol{\zeta}^\top \left[\mathbf{B}_f \,\text{sat}(\tilde{\mathbf{u}}_f) + \mathbf{g} + \mathbf{d} + \mathbf{K}\mathbf{z}_2 - \mathbf{M}\boldsymbol{\xi} + \mathbf{B}_f \left(\tilde{\mathbf{u}}_f - \text{sat}(\tilde{\mathbf{u}}_f)\right)\right] \\
&= -\mathbf{z}_1^\top K\mathbf{z}_1 + \mathbf{z}_1^\top \left(\boldsymbol{\zeta} - \boldsymbol{\xi}\right) + \boldsymbol{\zeta}^\top \left[\mathbf{B}_f \,\tilde{\mathbf{u}}_f + \mathbf{g} + \mathbf{d} + \mathbf{K}\mathbf{z}_2 - \mathbf{M}\boldsymbol{\xi}\right] \\
&= -\mathbf{z}_1^\top K\mathbf{z}_1 - \mathbf{z}_1^\top \boldsymbol{\xi} + \boldsymbol{\zeta}^\top \left[\mathbf{B}_f \,\tilde{\mathbf{u}}_f + \mathbf{g} + \mathbf{d} + \mathbf{K}\mathbf{z}_2 - \mathbf{M}\boldsymbol{\xi} + \mathbf{z}_1\right].
\end{aligned} \tag{22}$$

If we choose $\tilde{\mathbf{u}}_f$ as the one given in (16), then (22) reduces to

$$\dot{W}_2(\mathbf{z}_1, \boldsymbol{\zeta}) = -\mathbf{z}_1^\top K\mathbf{z}_1 - \mathbf{z}_1^\top \boldsymbol{\xi} - \boldsymbol{\zeta}^\top \mathbf{N}\boldsymbol{\zeta} + \boldsymbol{\zeta}^\top \left(\mathbf{d} - \hat{\mathbf{d}}\right). \tag{23}$$

To ensure $\dot{W}_2 < 0$, we need to show that $-\mathbf{z}_1^\top K\mathbf{z}_1 - \boldsymbol{\zeta}^\top \mathbf{N}\boldsymbol{\zeta}$ in (23) dominates the rest of the terms. Thus, we rewrite (23) using Rayleigh inequality as

$$\begin{aligned}
\dot{W}_2(\mathbf{z}_1, \boldsymbol{\zeta}) &\leq -\lambda_{\max}(K) \left\|\mathbf{z}_1\right\|_2^2 - \lambda_{\max}(N) \left\|\boldsymbol{\zeta}\right\|_2^2 - \left\|\mathbf{z}_1\right\|_2 \left\|\boldsymbol{\xi}\right\|_2 + \left\|\boldsymbol{\zeta}\right\|_2 \left\|\left(\mathbf{d} - \hat{\mathbf{d}}\right)\right\|_2 \\
&\leq -\left\|\mathbf{z}_1\right\|_2 \left(\lambda_{\max}(K) \left\|\mathbf{z}_1\right\|_2 - \left\|\boldsymbol{\xi}\right\|_2\right) - \left\|\boldsymbol{\zeta}\right\|_2 \left(\lambda_{\max}(N) \left\|\boldsymbol{\zeta}\right\|_2 - \left\|\left(\mathbf{d} - \hat{\mathbf{d}}\right)\right\|_2\right).
\end{aligned} \tag{24}$$

It readily follows from (24) that the decrement of W_2 is guaranteed outside the compact set, Ω as given in (19), that is

$$\dot{W}_2(\mathbf{z}_1, \boldsymbol{\zeta}) \leq -\lambda_{\max}(K) \left\|\mathbf{z}_1\right\|_2^2 - \lambda_{\max}(N) \left\|\boldsymbol{\zeta}\right\|_2^2 < 0; \; \forall\, \mathbf{z}_1, \boldsymbol{\zeta} \neq \mathbf{0}. \tag{25}$$

Clearly, the system trajectories of (14) converge to Ω asymptotically and remain uniformly bounded within it. Within Ω, the ultimate performance bound can be obtained by evaluating the maximum of W_2 within Ω, such that

$$W_1(\mathbf{z}_1) < W_2(\mathbf{z}_1, \boldsymbol{\zeta}) < \max_{(\mathbf{z}_1, \boldsymbol{\zeta}) \in \Omega} W_2(\mathbf{z}_1, \boldsymbol{\zeta}) = \max_{(\mathbf{z}_1, \boldsymbol{\zeta}) \in \Omega} \left[\frac{1}{2}\left(\frac{\boldsymbol{\xi}}{\lambda_{\max}(K)}\right)^2 + \frac{1}{2}\left(\frac{\mathbf{d} - \hat{\mathbf{d}}}{\lambda_{\max}(N)}\right)^2\right]. \tag{26}$$

From (26), it is apparent that the ultimate performance bound is indeed given by (20). This concludes the proof. □

Remark 2. One may notice from (26) that $\boldsymbol{\xi}$ and $\hat{\mathbf{d}}$ are critical in deciding the ultimate performance bound on the system trajectories of (14). To further elucidate this, consider a scenario where the follower's control law respects the saturation constraints, and the information about $\mathbf{d}$ is perfect; that is, both $\tilde{\mathbf{u}}_f - \text{sat}(\tilde{\mathbf{u}}_f)$ and $\mathbf{d} - \hat{\mathbf{d}}$ are zero. Consequently, $\boldsymbol{\xi} \to 0$ asymptotically whose rate of convergence can be dictated by choosing a suitable $\mathbf{M}$, which in turn, would lead to

asymptotic convergence of $\mathbf{z}_1$, $\mathbf{z}_2$, and $\boldsymbol{\zeta}$.

It is also worth mentioning that if $\boldsymbol{\xi}$ does not vanish, then the said leader-follower ring formation may not be guaranteed. For example, when the follower is initially located too far from the leader/ring such that $\mathbf{e}$ is large, its control efforts may become saturated. If this saturation persists indefinitely, then $\boldsymbol{\xi}$ does not vanish, thereby leading to failure of the desired ring formation. However, in most cases, it is reasonable to assume that the follower's control efforts are not saturated, at least after a finite time. Thus ring formation may be achieved since $\boldsymbol{\xi}$ will eventually decrease to zero. In the interest of proposing a new flexible formation scheme, we assume that the leader-follower engagement does not lead to the follower's control inputs saturating indefinitely. We leave an in-depth investigation of feasible geometries for ring formation for our future work.

C. Effects of Saturation on the Follower's Control Efforts

In the previous subsection, we designed $\tilde{\mathbf{u}}_f$ to stabilize (14). Since $\tilde{\mathbf{u}}_f$ and the follower's actual control effort, $\mathbf{u}_f$, are related through (15), we finally consider the input saturation constraints to design $\mathbf{u}_f$. Note that the mapping between $\mathbf{u}_f$ and $\tilde{\mathbf{u}}_f$ is nonlinear. Further, steering the follower using thrust, load factor, and bank angle while considering saturation constraints requires solving an energy minimization procedure which may involve evaluating nonlinear objective functions or nonlinear constraints. To provide an appropriate representation of the follower's control inputs considering saturation constraints for the proposed ring formation scenario, we propose to use nonlinear programming instead of directly saturating thrust, load factor, and bank angle. Specifically, we minimize the difference between the available and the demanded control efforts. The nonlinear programming routine used in our paper takes the load factor and the bank angle as inputs and provides their suitable values as outputs to constrain them within their desired physical limits. In order to perform the necessary computations, the routine iterates several times until the desired values at the output are achieved.

Consider the following minimization procedure where we obtain the load factor and the bank angle within their permissible limits, given by

$$\begin{aligned}\left(n_f^\star, \phi_f^\star\right) &= \underset{\substack{n_{f_{\min}} \le n_f \le n_{f_{\max}} \\ \phi_{f_{\min}} \le \phi_f \le \phi_{f_{\max}}}}{\arg\min} \quad \left(\mathrm{sat}(\tilde{u}_{f_2}) - \tilde{u}_{f_2}\right)^2 + \left(\mathrm{sat}(\tilde{u}_{f_3}) - \tilde{u}_{f_3}\right)^2 \\ &= \underset{\substack{n_{f_{\min}} \le n_f \le n_{f_{\max}} \\ \phi_{f_{\min}} \le \phi_f \le \phi_{f_{\max}}}}{\arg\min} \quad \left(\mathrm{sat}(\tilde{u}_{f_2}) - n_f \cos\phi_f\right)^2 + \left(\mathrm{sat}(\tilde{u}_{f_3}) - n_f \sin\phi_f\right)^2 . \end{aligned} \tag{27}$$

In (27), we do not include the $\tilde{u}_{f_1}$ mainly because it contains terms representing the follower's thrust and drag, whose minimum values together with $n_f^\star$, $\phi_f^\star$, may not represent their actual physical values. Instead, once the load factor and the bank angle are obtained, the required value of thrust can be evaluated using (15), (27) and an indicator variable $\mathcal{I}$, such that

$\mathcal{I} = m\tilde{u}_{f_1} + D_f(n_f^\star)$. Depending on $\mathcal{I}$, we have $T_f^\star = \begin{cases} \max\left(T_{\min}, \min\left(T_{\max}, \mathcal{I}\right)\right) & \text{if } \mathcal{I} \geq 0, \\ \max\left(0, \min\left(1, -\dfrac{\mathcal{I}}{D_{\mathcal{B}}}\right)\right);\ D_{\mathcal{B}} = \dfrac{1}{2}\rho S_f V_f^2 C_{d_{\mathcal{B}}} & \text{if } \mathcal{I} < 0. \end{cases}$. Since the thrust is non-negative in practice, we introduce an airbrake, $\mathcal{B}$, which is represented as $\mathcal{B} = \max\left(0, \min\left(1, -\dfrac{\mathcal{I}}{D_{\mathcal{B}}}\right)\right)$, where $C_{d_{\mathcal{B}}}$ is the airbrake coefficient which helps reverse the thrust value when $\mathcal{I}$ becomes negative.

IV. Simulations

This section validates the proposed results on Cessna 172 Skyhawk [40], which is a fixed-wing aircraft. We demonstrate the efficacy of the proposed control law in achieving ring formation around the leader, which makes independent loiter and straight-line maneuvers. The leader, whose initial position is $[0, -635, -1000]^\top$ m in the inertial frame, moves with an initial speed of 60 m/s with zero initial flight path and bank angles. We consider the radius of the ring as 30 m whose center in the leader's body frame is $[30, 0, 0]^\top$ m. Other parameters used in simulation are presented in Table 1. Initially, $\phi = 0°$ and $n = 1$ are used as the guess for the nonlinear programming routine.

Table 1 Simulation parameters.

Parameter	Value	Unit	Parameter	Value	Unit
m_k	1111	kg	$[K_{11}, K_{22}, K_{33}]$	0.1	-
ρ_k	1.225	kg/m^3	$[M_{11}, M_{22}, M_{33}]$	0.1	-
g	9.81	m/s^2	$[N_{11}, N_{22}, N_{33}]$	20	-
A_{r_k}	7.32	-	κ	0.1	-
A_k	16.2	m^2	T_f	[0, 2000]	N
η_k	0.85	-	$\mathcal{B}$	(0, 1)	-
$C_{d_{0_k}}$	0.01	-	n_f	[0, 2]	-
$C_{d_{\mathcal{B}}}$	0.02	-	ϕ_f	$\left[-\frac{\pi}{3}, \frac{\pi}{3}\right]$	rad

Fig. 3 depicts the follower achieving and maintaining ring formation behind the leader when the latter executes loiter maneuver. The follower's initial speed and heading are the same as that of the leader whereas its initial position in inertial frame is $[-100, -735, -1100]^\top$ m. Since the leader is in steady loiter maneuver, its control inputs are constant, that is, $\mathbf{u}_l = [584.04\text{N}, 1.1547, 30°]^\top$.

The trajectories of the leader and the follower are shown in Fig. 3a, where we can observe that the follower is able to converge to the ring and maintains ring formation for all future times. For a loiter maneuver, the linear speed is inversely proportional to the loiter radius, therefore less thrust is required by an aircraft for a smaller loiter radius. It can be seen Fig. 3a that the radius of the follower's loiter circle is smaller that that of the leader. Therefore, the follower will consume less thrust to maintain formation in steady state. We have also demonstrated a scenario wherein the follower converges to the nearest point on the ring. Note that converging to the nearest point on the ring does not necessary lead

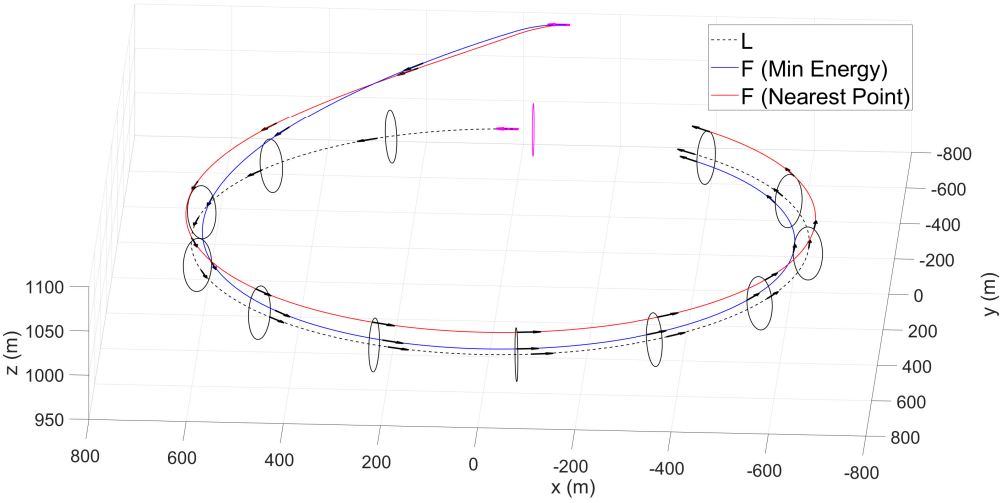

(a) Trajectories.

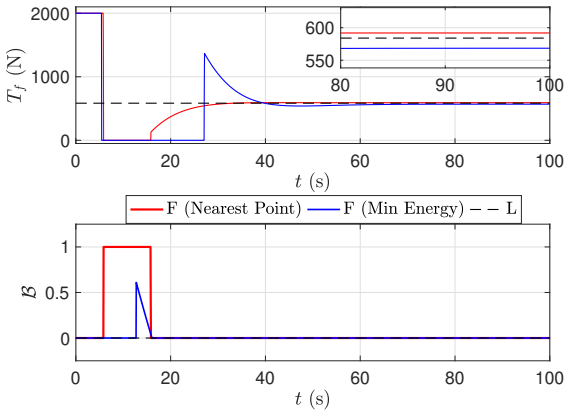

(b) Thrust and airbrake.

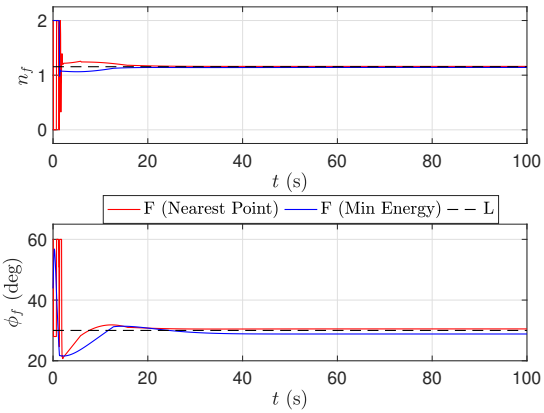

(c) Load factor and bank angle.

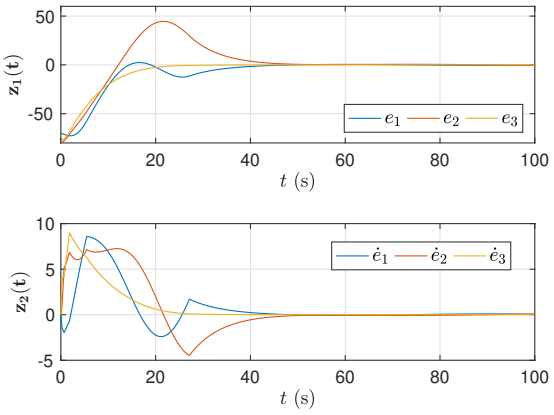

(d) Position and velocity errors.

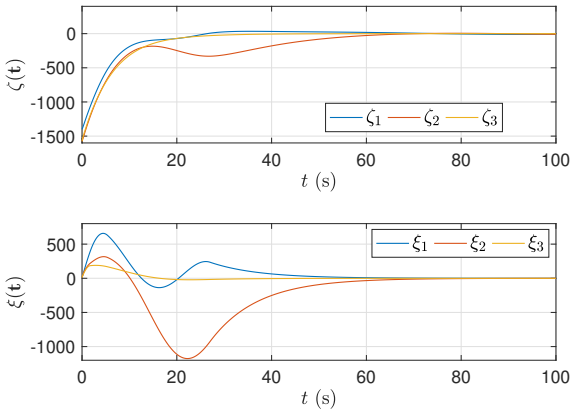

(e) Convergence of $\boldsymbol{\zeta}$ and $\boldsymbol{\xi}$.

Fig. 3 The follower's ring formation when the leader executes loiter maneuver.

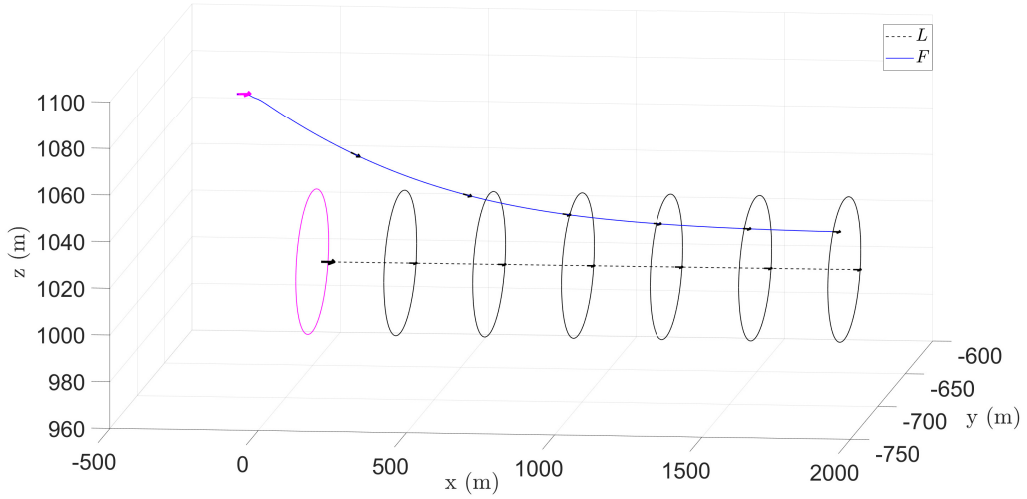

(a) Trajectories.

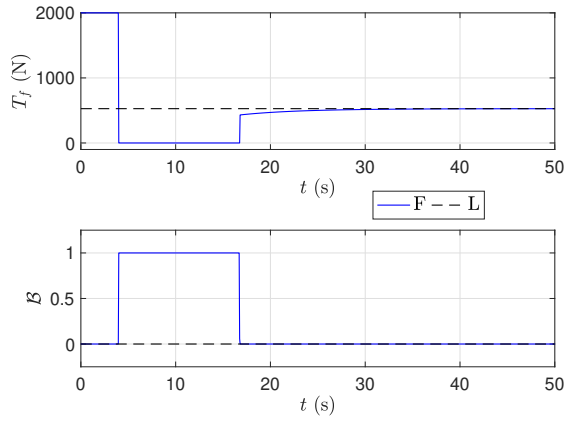

(b) Thrust and airbrake.

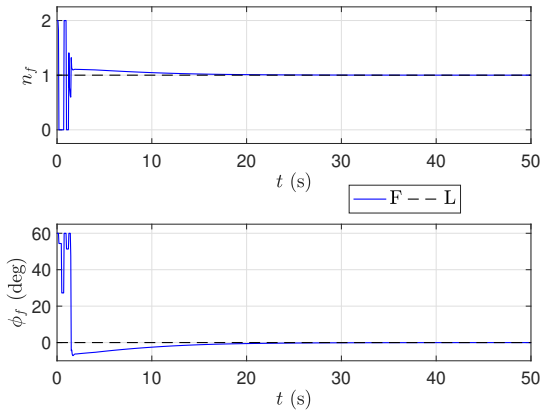

(c) Load factor and bank angle.

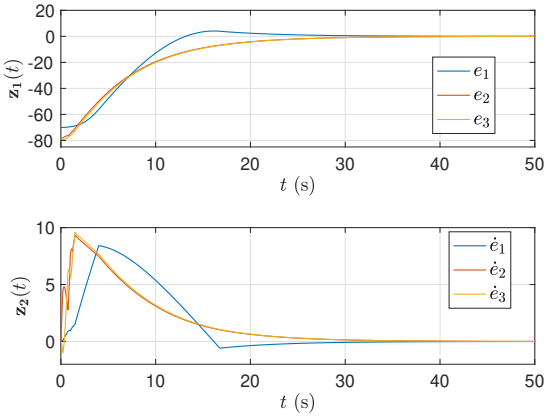

(d) Position and velocity errors.

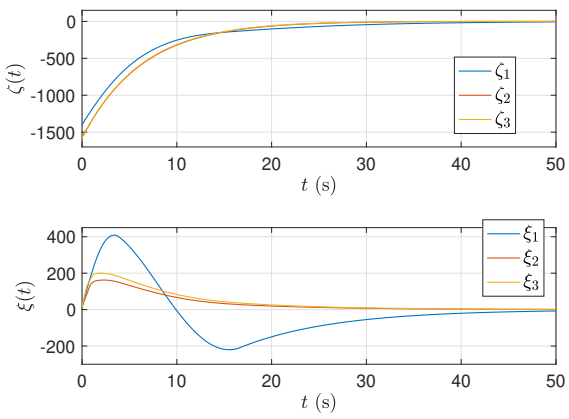

(e) Convergence of $\boldsymbol{\zeta}$ and $\boldsymbol{\xi}$.

Fig. 4 The follower's ring formation when the leader executes straight-line maneuver.

to an energy-efficient formation unless the leader is moving in a straight-line. The variation of the follower's control inputs are depicted in Figs. 3b–3c. Thrust and airbrake are responsible for controlling the follower's forward motion. Notice that the airbrake input, shown in Fig. 3b, activates only when the thrust demand is non-positive. Without a mechanism to provide negative thrust, the follower's controller will overshoot. The load factor and the bank angle, shown in Fig. 3c, also remain within their permissible limits during the entire formation maneuver.

The profiles of various error variables are also shown in Figs. 3d–3e, which evidence that after a short transient phase, the errors asymptotically tend to zero under the action of the follower's control inputs. Owing to the control affine treatment of the second-order error dynamics, the errors exhibit slow oscillatory behavior initially before asymptotically decaying to zero. During this time, the control efforts reduce in magnitude before settling down at a fixed value.

A similar discussion follows for the case when the leader moves in a straight line. Keeping the initial conditions same as before, Fig. 4 illustrates the follower's ring formation maneuver when the leader moves in a straight line. Since the leader is moving in straight line, its control inputs are constant, that is, $\mathbf{u}_l = [527.33\text{N}, 1.0, 0^\circ]^\top$. In this case, the follower's nearest point on the ring, $\mathcal{P}_n$, is the point that corresponds to minimum energy. As the error variables converge, the follower's control effort also reduce, eventually keeping the follower on the ring. The necessary error variables and the control effort follow a similar trend as those in the previous case of the leader's loiter maneuver.

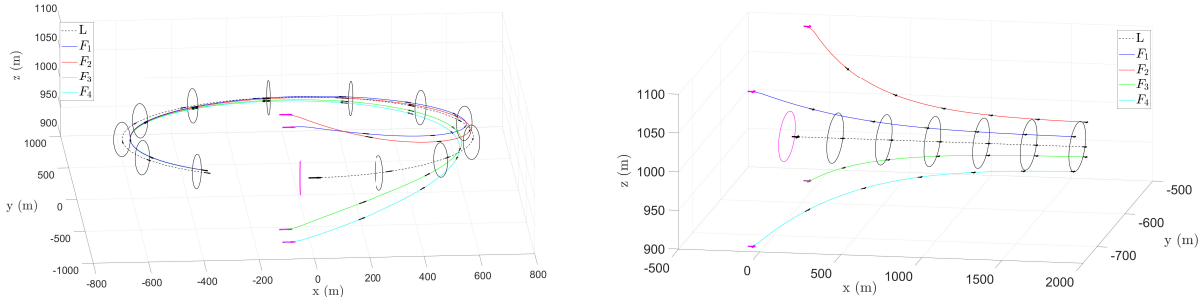

(a) The leader moves in a loiter circle. **(b) The leader moves in a straight line.**

Fig. 5 The follower's trajectories for various initial conditions.

We also demonstrate the follower's trajectories under various initial conditions when the leader executes loiter and straight-line maneuvers. These different initial positions of the follower are denoted as F_1 through F_2 such that $F_1 = [-100; -735; -1100]^\top$ m, $F_2 = [-100; -535; -1100]^\top$ m, $F_3 = [-100; -535; -900]^\top$ m, and $F_4 = [-100; -735; -900]^\top$ m. The leader's initial conditions and control inputs remain the same as before depending on the maneuver it executes. Fig. 5a shows that the follower, starting at different initial positions, converges to the same point on the ring which is the minimum energy point when the leader executes loiter maneuver. When the leader is moving in a straight line, the follower converges to different points on the ring nearest to its initial position as seen in Fig. 5b.

Fig. 6a shows the ring angles corresponding to the $\mathcal{P}^\star$ in the leader's frame, and the follower's nearest point on the ring. It is observed that the instantaneous value of the ring angle, as seen by the follower, eventually tracks the actual

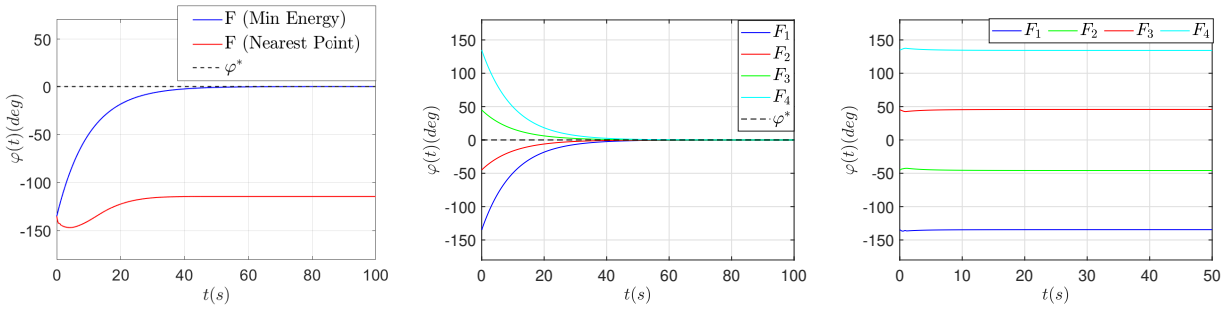

(a) Ring angle comparison when leader in loiter. **(b) Leader executes loiter maneuver.** **(c) Leader moves in straight line.**

Fig. 6 Ring angles for various initial conditions.

value of $\varphi^\star$ after the necessary error variables have converged (when the leader is in loiter). However, the follower converges to the same ring angle with respect to the leader in the case of the leader's loiter maneuver, as seen in Fig. 6b. For the straight-line maneuver, all the points on the ring experience the same velocity, thus the follower converges to the nearest point on the ring depending on its initial position (see Fig. 6c).

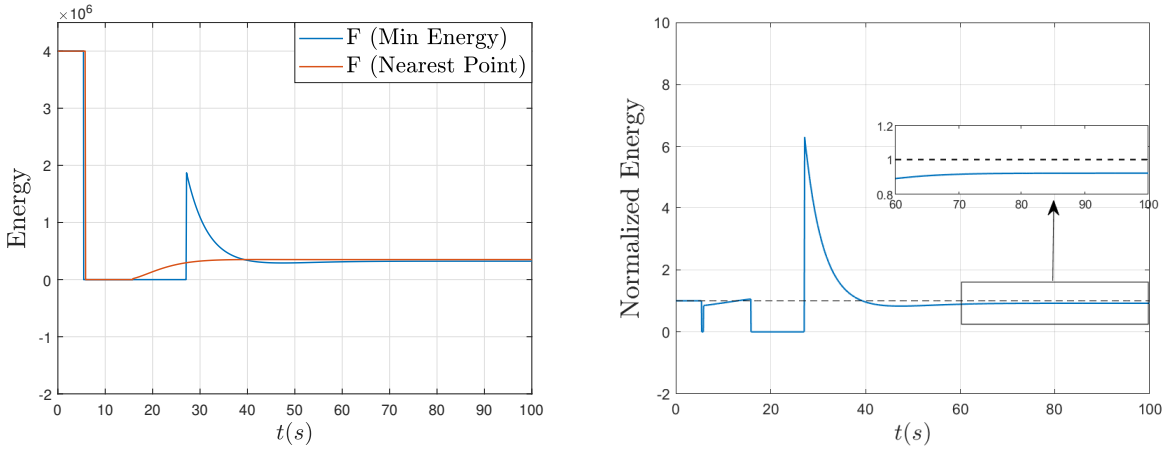

(a) Energy expenditure corresponding to $\mathcal{P}^\star$ and $\mathcal{P}_n$. **(b) Normalized energy expenditure.**

Fig. 7 The follower's energy expenditure for the leader's loiter maneuver.

A comparison of overall control effort, computed using $\int_0^t \mathbf{u}^\top \mathbf{u}\, dt$, is also depicted in Fig. 7 where we have normalized the follower's control effort (when it converges to $\mathcal{P}^\star$) with respect to that corresponding to any other point on the ring (for example, $\mathcal{P}_n$). Clearly, the proposed control law demands less energy in the steady-state. The initial increase in control effort may be attributed to the fact that the follower is trying to reach $\mathcal{P}^\star$, so it has to take necessary maneuvers before its energy requirements could be reduced. For a typical loiter maneuver of the leader, it can be observed that the follower demands 8% less energy to converge to the ring if it is steered on $\mathcal{P}^\star$ as compared to the nearest point on the ring.

We now show the Monte Carlo simulations to attest to the merits of the proposed technique. From Fig. 8a, it is

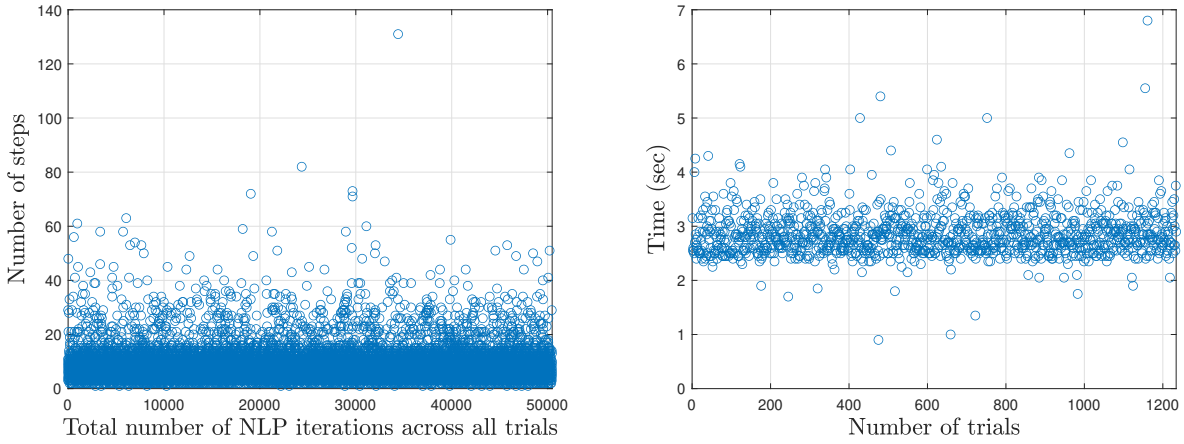

(a) NLP convergence rate. **(b) Time required for saturation depletion.**

Fig. 8 Monte Carlo simulations related to the convergence of nonlinear programming routine.

evident that for an experiment repeated around 1200 times with arbitrary initial conditions, the nonlinear programming routine converges within 60 steps. On the other hand, it can be observed from Fig. 8b that it takes around 4-5 seconds for the saturated values of the corresponding variables to vanish. Thereafter, the routine may not be needed since the load factor, and the bank angle never hit the saturation limits.

V. Conclusions and Future Work

This paper presented an energy-efficient flexible formation scheme for a leader-follower aircraft system, namely ring formation. Such a formation is a set of desired points around the leader where the follower might choose to converge and stay at regardless of the leader's maneuvers. The proposed method accounted for aerodynamic parameter variation through suitable control inputs, which were constrained in the design due to their physical limitations. The follower was steered to a specific point on the ring, using thrust, load factor, and bank angle, which corresponds to the minimum energy expenditure. The proposed design was based on the backstepping technique, where we proved the ultimate boundedness of the system trajectories when the effects of control input saturation were accounted for. Owing to the nonlinear constraints in the saturated control design, we used nonlinear programming to obtain the follower's actual control inputs. From a comparison of the follower's normalized energy expenditure in various scenarios, it was inferred that the follower demands lesser energy when it converges to the point that corresponds to the minimum speed point. However, it expended more energy even if it had to converge to the nearest point on the ring. The current results may be extended to account for the time-varying radius of the ring or even to a more generalized shape behind the leader (e.g., an ellipse or a sphere). Further, casting the same problem as an energy minimization one to steer the follower on the ring may offer a different perspective to look at the same problem in the future. Incorporating multiple followers within an energy-efficient formation framework could be another interesting direction to pursue in the future.

Acknowledgments

This work was supported in part by the Air Force Research Lab under Grant FA8650-20-2-2419 and the Office of Naval Research under Grant N00014-19-1-2278.

References

[1] Frew, E. W., "Sensitivity of Cooperative Target Geolocalization to Orbit Coordination," *Journal of Guidance, Control, and Dynamics*, Vol. 31, No. 4, 2008, pp. 1028–1040. https://doi.org/10.2514/1.32810.

[2] Yang, J., Yin, D., Niu, Y., and Shen, L., "Distributed Cooperative Onboard Planning for the Conflict Resolution of Unmanned Aerial Vehicles," *Journal of Guidance, Control, and Dynamics*, Vol. 42, No. 2, 2019, pp. 272–283. https://doi.org/10.2514/1.G003583.

[3] Sinha, A., Kumar, S. R., and Mukherjee, D., "Three-Dimensional Nonlinear Cooperative Salvo Using Event-Triggered Strategy," *Journal of Guidance, Control, and Dynamics*, Vol. 44, No. 2, 2021, pp. 328–342. https://doi.org/10.2514/1.G005367.

[4] Cao, Y., and Ren, W., "Distributed Coordinated Tracking With Reduced Interaction via a Variable Structure Approach," *IEEE Transactions on Automatic Control*, Vol. 57, No. 1, 2012, pp. 33–48. https://doi.org/10.1109/TAC.2011.2146830.

[5] Cao, Y., Ren, W., and Egerstedt, M., "Distributed containment control with multiple stationary or dynamic leaders in fixed and switching directed networks," *Automatica*, Vol. 48, No. 8, 2012, pp. 1586–1597. https://doi.org/10.1016/j.automatica.2012.05.071.

[6] Khalili, M., Zhang, X., Cao, Y., Polycarpou, M. M., and Parisini, T., "Distributed adaptive fault-tolerant leader-following formation control of nonlinear uncertain second-order multi-agent systems," *International Journal of Robust and Nonlinear Control*, Vol. 28, No. 15, 2018, pp. 4287–4308. https://doi.org/10.1002/rnc.4232.

[7] Gil, A. E., Passino, K. M., and Cruz Jr., J. B., "Stable Cooperative Surveillance With Information Flow Constraints," *IEEE Transactions on Control Systems Technology*, Vol. 16, No. 5, 2008, pp. 856–868. https://doi.org/10.1109/TCST.2007.916329.

[8] Subbarao, K., and Ahmed, M., "Target tracking using multiple unmanned aerial vehicles: Graph theoretic nonlinear control approach," *Proceedings of the Institution of Mechanical Engineers, Part G: Journal of Aerospace Engineering*, Vol. 231, No. 3, 2017, pp. 570–586. https://doi.org/10.1177/0954410016641321.

[9] Milutinović, D., and Casbeer, D. W., "Leader-Follower Formation Feedback Control Composed of Turning Rate and Velocity Controllers," *2020 International Conference on Unmanned Aircraft Systems (ICUAS)*, 2020, pp. 1189–1198. https://doi.org/10.1109/ICUAS48674.2020.9213868.

[10] Pachter, M., D'Azzo, J. J., and Dargan, J. L., "Automatic formation flight control," *Journal of Guidance, Control, and Dynamics*, Vol. 17, No. 6, 1994, pp. 1380–1383. https://doi.org/10.2514/3.21364.

[11] Tahk, M.-J., Park, C.-S., and Ryoo, C.-K., "Line-of-Sight Guidance Laws for Formation Flight," *Journal of Guidance, Control, and Dynamics*, Vol. 28, No. 4, 2005, pp. 708–716. https://doi.org/10.2514/1.9605.

[12] Campa, G., Wan, S., Napolitano, M. R., Seanor, B., and Fravolini, M. L., "Design of formation control laws for manoeuvred flight," *The Aeronautical Journal (1968)*, Vol. 108, No. 1081, 2004, p. 125–134. https://doi.org/10.1017/S0001924000151577.

[13] Barfoot, T., and Clark, C., "Motion planning for formations of mobile robots," *Robotics and Autonomous Systems*, Vol. 46, No. 2, 2004, pp. 65–78. https://doi.org/10.1016/j.robot.2003.11.004.

[14] Low, C. B., and Ng, Q. S., "A flexible virtual structure formation keeping control for fixed-wing UAVs," *2011 9th IEEE International Conference on Control and Automation (ICCA)*, 2011, pp. 621–626. https://doi.org/10.1109/ICCA.2011.6137876.

[15] Kownacki, C., and Ambroziak, L., "Flexible Structure Control Scheme of a UAVs Formation to Improve the Formation Stability During Maneuvers," *Acta Mechanica et Automatica*, Vol. 11, No. 3, 2017, pp. 178–185. https://doi.org/doi:10.1515/ama-2017-0026.

[16] Kim, Y., and Choi, J., "Fuel-Efficient Formation Flight-Control Design Based on Energy Maneuverability," *Journal of Guidance, Control, and Dynamics*, Vol. 31, No. 4, 2008, pp. 1145–1150. https://doi.org/10.2514/1.34351.

[17] Shestakov, S., Ivanov, D., and Ovchinnikov, M., "Formation-Flying Momentum Exchange Control by Separate Mass," *Journal of Guidance, Control, and Dynamics*, Vol. 38, No. 8, 2015, pp. 1534–1543. https://doi.org/10.2514/1.G001137.

[18] Yan, H., and Alfriend, K. T., "Approximate Minimum Energy Control Laws for Low-Thrust Formation Reconfiguration," *Journal of Guidance, Control, and Dynamics*, Vol. 30, No. 4, 2007, pp. 1182–1186. https://doi.org/10.2514/1.28494.

[19] Blahnick, D., *The Formation Pilots' Knowledge Guide*, 2012.

[20] Tran, D. M., Casbeer, D., Garcia, E., Weintraub, I. E., Milutinovic, D., and Manyam, S. G., "Ring Formation Maneuver: Single-Integrator Kinematics," *AIAA Scitech 2021 Forum*, 2021, pp. 1–12. https://doi.org/10.2514/6.2021-0978.

[21] Tran, D., Casbeer, D., Garcia, E., Weintraub, I. E., and Milutinović, D., "Ring Formation Maneuvering with Double Integrator Dynamics," *2021 International Conference on Unmanned Aircraft Systems (ICUAS)*, 2021, pp. 1580–1586. https://doi.org/10.1109/ICUAS51884.2021.9476770.

[22] Tran, D., Casbeer, D., Garcia, E., Weintraub, I. E., and Milutinović, D., "Ring Formation Maneuver: Double-Integrator Kinematics with Input Saturation," *Journal of Guidance, Control, and Dynamics*, Vol. 44, No. 11, 2021, pp. 2091–2098. https://doi.org/10.2514/1.G005925.

[23] Williamson, W. R., Abdel-Hafez, M. F., Rhee, I., Song, E.-J., Wolfe, J. D., Chichka, D. F., and Speyer, J. L., "An Instrumentation System Applied to Formation Flight," *IEEE Transactions on Control Systems Technology*, Vol. 15, No. 1, 2007, pp. 75–85. https://doi.org/10.1109/TCST.2006.883241.

[24] Dimock, G., and Selig, M., "The Aerodynamic Benefits of Self-Organization in Bird Flocks," *41st Aerospace Sciences Meeting and Exhibit*, 2003, pp. 1–9. https://doi.org/10.2514/6.2003-608.

[25] McCamish, S., Pachter, M., and D'Azzo, J., "Optimal formation flight control," *Guidance, Navigation, and Control Conference*, 1996, pp. 1–18. https://doi.org/10.2514/6.1996-3868.

[26] Veth, M., Pachter, M., and D'Azzo, J. J., "Energy preserving formation flight control," *33rd Aerospace Sciences Meeting and Exhibit*, 1995, pp. 1–9. https://doi.org/10.2514/6.1995-335.

[27] Ranjan, P., Votion, J., Cao, Y., Tran, D. M., Casbeer, D., and Weintraub, I. E., "Energy-aware 3D Leader-Follower Flight Trajectory Optimization for Fixed-Wing Aircraft," *AIAA SCITECH 2022 Forum*, 2022, pp. 1–17. https://doi.org/10.2514/6.2022-2217.

[28] Anderson, J. D., and Bowden, M. L., *Introduction to Flight*, McGraw-Hill Higher Education New York, 2005.

[29] Raymer, D., *Aircraft Design: A Conceptual Approach*, American Institute of Aeronautics and Astronautics, Inc., 2012. https://doi.org/10.2514/6.2008-7172.

[30] Sinha, A., Kumar, S. R., and Mukherjee, D., "Three-Dimensional Guidance with Terminal Time Constraints for Wide Launch Envelops," *Journal of Guidance, Control, and Dynamics*, Vol. 44, No. 2, 2021, pp. 343–359. https://doi.org/10.2514/1.G005180.

[31] Elston, J., and Frew, E., "Unmanned Aircraft Guidance for Penetration of Pretornadic Storms," *Journal of Guidance, Control, and Dynamics*, Vol. 33, No. 1, 2010, pp. 99–107. https://doi.org/10.2514/1.45195.

[32] Sinha, A., Kumar, S. R., and Mukherjee, D., "Three-agent Time-constrained Cooperative Pursuit-Evasion," *Journal of Intelligent & Robotic Systems*, Vol. 104, No. 2, 2022, p. 28. https://doi.org/10.1007/s10846-022-01570-y.

[33] Shima, T., Idan, M., and Golan, O. M., "Sliding-Mode Control for Integrated Missile Autopilot Guidance," *Journal of Guidance, Control, and Dynamics*, Vol. 29, No. 2, 2006, pp. 250–260. https://doi.org/10.2514/1.14951.

[34] Sinha, A., and Kumar, S. R., "Supertwisting Control-Based Cooperative Salvo Guidance Using Leader–Follower Approach," *IEEE Transactions on Aerospace and Electronic Systems*, Vol. 56, No. 5, 2020, pp. 3556–3565. https://doi.org/10.1109/TAES.2020.2974044.

[35] Shima, T., "Optimal Cooperative Pursuit and Evasion Strategies Against a Homing Missile," *Journal of Guidance, Control, and Dynamics*, Vol. 34, No. 2, 2011, pp. 414–425. https://doi.org/10.2514/1.51765.

[36] Sinha, A., Kumar, S. R., and Mukherjee, D., "Impact time constrained integrated guidance and control design," *Aerospace Science and Technology*, Vol. 115, 2021, p. 106824. https://doi.org/10.1016/j.ast.2021.106824.

[37] Garcia, E., Casbeer, D. W., and Pachter, M., "Cooperative Strategies for Optimal Aircraft Defense from an Attacking Missile," *Journal of Guidance, Control, and Dynamics*, Vol. 38, No. 8, 2015, pp. 1510–1520. https://doi.org/10.2514/1.G001083.

[38] Tran, D., Casbeer, D., Garcia, E., Weintraub, I. E., and Milutinović, D., "Ring Formation Maneuver: Double-Integrator Kinematics with Input Saturation," *Journal of Guidance, Control, and Dynamics*, Vol. 44, No. 11, 2021, pp. 2091–2098. https://doi.org/10.2514/1.G005925.

[39] Farrell, J. A., Polycarpou, M., Sharma, M., and Dong, W., "Command Filtered Backstepping," *IEEE Transactions on Automatic Control*, Vol. 54, No. 6, 2009, pp. 1391–1395. https://doi.org/10.1109/TAC.2009.2015562.

[40] Cessna, "Cessna Skyhawk Performance," , 2009. URL https://web.archive.org/web/20100814150916/http://cessna.com/single-engine/skyhawk/skyhawk-performance.html.